HMG Advance Access published February 3, 2009

The Multimeric Structure of Polycystin-2 (TRPP2): Structural-Functional Correlates of Homo- and Hetero-multimers with TRPC1

Peng Zhang[1], Ying Luo[3], Bernard Chasan[4], Silvia González-Perrett[2], Nicolás Montalbetti[2], Gustavo A. Timpanaro[2], María del Rocío Cantero[2], Arnolt J. Ramos[1], Wolfgang H. Goldmann[1], Jing Zhou[3], and Horacio F. Cantiello[1,2*]

[1]Nephrology Division & Electrophysiology Core, Massachusetts General Hospital East, Charlestown, MA, 02129 and Department of Medicine, Harvard Medical School, Boston, MA, 02115 USA

[2]Laboratorio de Canales Iónicos, ININCA, UBA-CONICET, Buenos Aires, 1122AAJ, Argentina

[3]Renal Division, Department of Medicine, Brigham's and Women's Hospital, and Harvard Medical School, Boston, MA, 02115 USA

[4]Physics Department, Boston University, Boston, MA, 02115

*Address correspondence to: Horacio F. Cantiello, Nephrology Division & Electrophysiology Core, Massachusetts General Hospital East, 149 13th Street, Charlestown, MA 02129, Tel: 617-7265640; Fax: 617-7265669; Email: cantiello@helix.mgh.harvard.edu

Abstract

Polycystin-2 (PC2, TRPP2), the gene product of *PKD2*, whose mutations cause autosomal dominant polycystic kidney disease (ADPKD), belongs to the superfamily of TRP channels. PC2 is a non-selective cation channel, with multiple subconductance states. In this report, we explored structural and functional properties of PC2 and whether the conductance substates represent monomeric contributions to the channel complex. A kinetic analysis of spontaneous channel currents of PC2 showed that four intrinsic, non-stochastic sub-conductance states, which followed a staircase behavior, were both pH-, and voltage-dependent. To confirm the oligomeric contributions to PC2 channel function, heteromeric PC2/TRPC1 channel complexes were also functionally assessed by single channel current analysis. Low pH inhibited the PC2 currents in PC2 homomeric complexes, but failed to affect PC2 currents in PC2/TRPC1 heteromeric complexes. Amiloride, in contrast, abolished PC2 currents in both the homomeric PC2 complexes and the heteromeric PC2/TRPC1 complexes, thus PC2/TRPC1 complexes have distinct functional properties from the homomeric complexes. The topological features of the homomeric PC2-, TRPC1-, and heteromeric PC2/TRPC1 channel complexes, assessed by atomic force microscopy (AFM), were consistent with structural tetramers. TRPC1 homomeric channels had different average diameter and protruding height as compared to the PC2 homomers. The contribution of individual monomers to the PC2/TRPC1 hetero-complexes was easily distinguishable. The data support tetrameric models of both the PC2 and TRPC1 channels, where the overall conductance of a particular channel will depend on the contribution of the various functional monomers in the complex.

Introduction

The gene product of *PKD2*, PC2, one of the genes implicated in ADPKD (31), belongs to the superfamily of TRP channels (34, 35). PC2 (36) is a large conductance, Ca^{2+}-permeable non-selective cation channel (20, 47), which is involved in Ca^{2+} transport (20, 32) and in Ca^{2+} signaling in renal epithelial cells (37). As most prototypical TRP channel proteins, PC2 is topologically organized in six transmembrane (6TM) domains, and cytoplasmic carboxy- and amino- termini (31). This topology, which is shared by a number of K^+ channels (28), is assembled such that a sensor region is expected in TMs 1-4, and a pore region, located in TMs 5-6, containing the P-loop. Based on their sequence similarities with the pore-forming α subunit of voltage-gated Ca^{2+} channels that contain four intra-molecular 6TM domains (9), TRP channels are expected to assemble as homo- and/or hetero-multimers, particularly potential tetramers. Similar assemblies have been found for the *Shaker* type K^+ channels (28) and cyclic nucleotide-gated (CNG) channels (26). Functional diversity by TRP channels is expected to lie in structural combinations of heterologous monomers. Hetero-multimerization by TRP channels was originally observed between *Drosophila* TRP and TRPL channels (49). The homo-tetrameric structure of the Ca^{2+}-permeable TRP channel TRPV6 (1, 16, 23, 44) and TRPC1 (7), for example, have been confirmed. Several 6TM containing voltage-gated and ligand-gated channels are also tetramers (15, 16, 22, 23, 39). Interestingly, the multimeric composition of a particular channel may correlate with its functional properties, including those reflected in the presence of functional subconductance states. The tetrameric glutamate receptor, for example, displays subconductance states, which are correlated with the subunit composition of the channel complex (39). Heteromeric assembly of TRP channels, including PC2 (13) may provide functional and regulatory diversity among channel complexes (21, 43, 49). PC2 is known to interact with TRPC1 (46), providing distinct functional properties to the channel complex (3). The PC2 channel often displays identical subconductance levels (32 pS) (20), representing an intrinsic property of PC2, as both endogenous PC2 from plasma membrane, and the *in vitro* transcribed/translated gene product, display similar functional features. Here, we determined that the conductive substates in PC2 and PC2/TRPC1 multimers are consistent with the individual contribution of monomers to the channel complex. Further, the formation of PC2/TRPC1 hetero-complexes renders distinct functional properties, such as resistance to low pH, only observed in TRPC1 homo-complexes, but not PC2 complexes. The topological structure of these channel complexes was confirmed by AFM, which showed that PC2 and TRPC1 homomers, as well as PC2/TRPC1 heteromers, assemble as structural tetramers. Functional diversity in both PC2 and TRPC1 may represent the individual ratio of the particular monomers composing the channel complex.

Results

Presence of subconductance states in PC2. Wild type PC2 single channel currents (Fig. 1) often display, spontaneous, short closures into either one of four most common subconductance states of identical amplitude (~32 pS, Figs. 1a-d) as originally reported (20). This is observed in the endogenous PC2 (Figs. 1a-c) from human syncytiotrophoblast and the *in vitro* translated gene product (Fig. 1d), indicating an intrinsic property of the PC2 channel. Upon full closure from its maximal conductance state, PC2 often re-opens in a staircase fashion, "climbing up" the increasing conductance levels, from previous conductance states (Fig. 1d). This phenomenon is both voltage-, and pH-dependent (Figs. 1e-f). An average of such spontaneous sojourns (n=9, from 5 experiments, Figs. 1e-f) shows a voltage-dependent staircase increase in conductance. Channel openings at 0 mV, showed discrete (~3.8 msec) semi-conductance delays not detected at 40 mV ($p<0.02$, n=7). Voltage dependence of the activation process also follows from voltage inactivation as recently reported (19) (data not shown). The lifetime of each occupancy state can also be modified by "protonation" of the channel (19) (Fig. 1f). This pH effect was also voltage dependent (Fig. 1f), suggesting that the protonation effect -itself- is voltage-dependent. The simplest interpretation of the data is consistent with the hypothesis that PC2 is a functional tetramer, whose conductance levels correspond to the sequential ("staircase") activation of each one of four "monomeric" units. According to this view, a fully functional channel requires the four subunits necessary for a complete channel opening. To confirm this view, the quaternary structure of the PC2 channel was determined by Western blot analysis after gel electrophoresis of affinity purified PC2 under both denaturing (Fig. 1g, Left, with SDS present) and non-denaturing (Fig. 1g, Right, without SDS) conditions. Large, 440 kDa (tetramers) and higher molecular weight complexes were preserved under non-denaturing conditions (Fig. 1g, Right), as compared to 110 kDa monomers under denaturing conditions (Fig. 1g, Left). Interestingly, 210 kDa complexes were also observed under denaturing condition (Fig. 1g, Left), which are most consistent with highly stable dimeric structures. An additional ~70 kDa band was detected under denaturing conditions, which is in agreement with previous reports by us and others using different antibodies (12, 33, 45, 48). This suggests that the smaller band could be a degraded (cleaved?) form of PC2 but not due to the non-specific recognition of the antibody.

Electrophysiological features of TRPC1 and TRPC1/PC2 complexes. To disclose the individual contribution of the various monomers in PC2 to the single channel conductance of the complex, we explored replacing PC2 subunits with TRPC1 monomers. The electrical properties of the TRPC1 channel were first determined in the homomeric complex. Reconstituted TRPC1 displayed a single channel conductance of 5.0 ± 0.7 pS (n=5) in the presence of a KCl chemical gradient (Figs. 2a-b, 150 *vs* 15 mM K^+ for *cis* and *trans* chambers, respectively). TRPC1 channels also displayed a 22.8 ± 2.0 pS (n=5) conductance (Fig. 2b), consistent with a functional tetramer. The TRPC1 tetramer showed on occasion four subconductance states (Figs. 2c-d), consistent with four units of the 5 pS small channel shown in Fig 2b. Two features, which contrast with those previously observed with the PC2 channel (19, 20), included the fact that the TRPC1 homomeric channels were insensitive to both amiloride (200 μM, *trans* side, n=10, Fig. 2e) and low cytoplasmic pH (6.4-5.9, *cis* side, n=7, Fig. 2f). Owing to these functional differences, TRPC1/PC2 channel monomers were mixed and reconstituted at equimolar ratios (1:1, w:w) in a lipid bilayer reconstitution chamber (Figs. 3-5). The electrophysiological properties of the PC2/TRPC1 hetero-complexes were quite distinct, and different from any of the homo-complexes of either type (Figs. 1 & 2). PC2-mediated single channel deflections were easily identifiable by their large

conductance compared to the smaller TRPC1 (~5 pS *vs.* 32 pS, respectively, Fig. 3). In most experiments (Figs. 4 & 5), the deflections also showed striking differences, including much higher open probability for the TRPC1 contribution, while fast flickering of the open state in the PC2 components of the channel. The single channel conductance of the PC2/TRPC1 hetero-complex (Figs. 3d-e) was intermediate between the conductances of PC2 (19) and TRPC1 homomers (Fig. 2b). Most interestingly, the data of single channel current deflections at various voltages suggests that a subpopulation of PC2/TRPC1 channel complexes behaved, in average, as TRPC1 homomers. In Fig. 3d, the blue line and triangles are the fitted data to a subpopulation of TRPC1/PC2 complexes, while the green line shows the fitted I-V relationship for TRPC1 homomers as shown in Fig. 2b. The conductance of this subpopulation of TRPC1/PC2 complexes was very close to that of TRPC1 homomers. The remainder TRPC1/PC2 complexes had a single channel conductance of 55.8 ± 2.9 pS (n=22, Fig. 3d, red lines and circles), which is only 35% of that observed for the PC2 homomer (Fig. 3d, grey line, 157 ± 4.9, n=7, $p<0.001$, d.f.=27). This conductance is, however, 245% higher than that of TRPC1 alone (Fig. 3d, green line, 22.8 ± 2.0 pS, n=5, $p<0.001$, d.f.=25). There also is a voltage dependent shift in conductance, at higher potentials (+60 to +150 mV in the reconstitution setup), such that the complex has a conductance of 53.7 ± 4.8 pS (n=7, Fig. 3d, red linear line), while the extrapolated conductance for the same complex at those same potentials would be 122 pS. This would suggest that the TRPC1 contribution to the channel may close at higher potentials, to let the PC2 components of the channel prevail (Fig. 3d, the red linear line at higher potentials). The distinct contribution of either component was further defined by addition of either amiloride (200 μM, *trans* side, Fig. 4) or 1.0 N HCl (*cis* side, Fig. 5) to lower the pH to 5.9 was used to modify the single channel currents of PC2 subunit in the functional hetero-complex. Interestingly, while amiloride addition blocked the PC2, but not the TRPC1 contribution to the PC2/TRPC1 complex (Fig. 4, n=7), lowering the pH was without effect on the overall hetero-complex conductance (Fig. 5, n=7). This evidence indicates that while the PC2/TRPC1 channel contains functional units of each contributing protein, the presence of TRPC1 in the hetero-complex renders the contributing PC2 refractory to low pH.

Topology of the PC2 and TRPC1 homomeric complexes. To identify the topological structure of the PC2/TRPC1 channels, the affinity-purified proteins were inserted into liposomes as for the electrophysiological studies. The reconstituted proteins were then imaged in solution by scanning flattened PC2-containing liposomes onto freshly cleaved mica with an atomic force microscope (Fig. 6). The topological structure of the PC2 channel showed the contribution of four monomers (Figs. 6a-c). PC2 channels were identified as bell-shaped structures with a 135 ± 3.38 nm diameter (n=107, mean ± SEM), and an average height of 1.21 ± 0.05 nm (n=107, Fig. 6d). A distribution of the diameter population (Fig. 6e) was consistent with a sharp peak at 116 ± 1.9 nm (n=61, the most likely monomeric contributor to the tetramer), and a wider, larger population of 163 ± 2.0 nm (n=46). The height showed a trimodal population with means of 0.73 ± 0.01 nm (n=43), and a higher population at 1.23 ± 0.01 nm (n=46). A few instances of approximately 1.81 ± 0.02 nm heights (n=18) were also observed, which are consistent with channel proteins bound to, but not inserted in the lipid bilayer. The PC2 monomers in the homomeric channel complexes were further identified by exposure to an anti-PC2 antibody (Catalog #52-5217, Zymed, South San Francisco, CA), which increased both the height and diameter of the complex (Fig. 7). Conversely, a decrease of the sample's pH by addition of HCl modified the topology of the PC2 channel complex, such that the different PC2 complexes had a reduced diameter compared to controls (Fig. 8). The calculated volume of the PC2 homomeric channel was 3663 ± 139 nm^3 (n=97). This value

was the peak obtained from a population analysis of molecular volumes (Figs. 10a-b) calculated for heights lower than 2 nm. The weak linear correlation for the height vs. diameter (Fig. 10a) indicates that the complexes evaluated for measurement were inserted and not apposed to the membrane. The distribution of the population indicates step-growth type polymerization of higher molecular weight complexes as well.

The topological structure of the homomeric TRPC1 channel was also determined by AFM imaging of affinity purified, reconstituted protein, which was carried out by scanning flattened TRPC1-containing liposomes onto freshly cleaved mica in solution (Fig. 9). TRPC1 channels were identified as multi-lobular structures with an average diameter of 49.3 ± 1.5 nm (n=105, mean ± SEM), and an average height of 3.1 ± 0.1 nm (n=105) (Fig. 9d). A distribution of the diameter population was consistent with a sharp peak at 32.3 nm ± 0.7 (n=37), and a wider, larger population of 51.6 ± 1.5 nm (n=68) (Fig. 9e). The height also showed a multimodal population with means of 2.1 ± 0.1 nm (n=53) and 3.6 ± 0.04 nm (n=41) (Fig. 9f). A few instances of approximately 5.8 nm heights (n=11) were also observed, which are consistent with channel proteins bound but not inserted in the lipid bilayer (Fig. 9f). The topology of the TRPC1 channel was consistent with a tetrameric complex (Fig. 9b-c). The calculated volume for the TRPC1 channel complex (Figs. 10c-d) was 1053 ± 51 nm^3 (n=94), remarkably different from that observed for the PC2 channel. The same criteria were used for data analysis of TRPC1 complexes. However, excluded heights for volume calculations were higher than 5 nm.

Topology of the PC2/TRPC1 hetero-complexes. To identify the topological structure of the PC2/TRPC1 hetero-complexes, affinity purified PC2 was mixed in a 1:1 ratio with affinity purified TRPC1, in identical mixture to that previously tested in the electrophysiological studies. PC2/TRPC1 channel complexes were incorporated into liposomes of same lipid composition used in the lipid bilayer studies. The reconstituted channel complexes were imaged in solution by scanning flattened PC2/TRPC1-containing liposomes onto freshly cleaved mica (Fig. 11). PC2/TRPC1 complexes were identified as lax, asymmetrical structures (Figs. 11a-b), where both the PC2 and TRPC1 monomers could be identified by height in the channel complexes. Consistent with the mixing ratio, most channel complexes had a tetrameric topology, with two PC2 monomers, and two TRPC1 monomers in each (Figs. 11b-c, circles). TRPC1 homo-complexes (squares) and PC2 homo-complexes (hexagons) could also be identified (Fig. 11b). The 2:2 PC2/TRPC1 hetero-complexes had, in average, an overall diameter of 129 ± 3.6 nm (n=12), which is between that of the homomeric PC2 complexes (163 ± 2.0 nm, Fig. 6e) and homomeric TRPC1 complexes (51.6 ± 1.5 nm, Fig. 9e). The contributing monomeric PC2 and TRPC1 in the hetero-complexes showed different height as expected (Fig. 11c), but their monomeric diameters were indistinguishable from each other, which were 43.7 ± 2.71 nm (n=9) *vs.* 45.3 ± 2.07 nm (n=9), respectively (Fig. 11c). Interestingly, the PC2 monomeric diameter in the PC2/TRPC1 hetero-complexes was greatly decreased comparing with that in the PC2 homo-complexes, suggesting that interaction between molecules (PC2-PC2 and PC2-TRPC1) may greatly affect their topological dimension outside the membrane, which, however, needs further studies to confirm.

Discussion

The members of the TRP superfamily of cation channels play diverse physiological roles, including receptor- and store-operated Ca^{2+} entry, mineral absorption, cell death, and particularly as sensors for pain, heat, cold, sound, stretch, and osmotic changes etc. The wide variety of physiological functions, in which TRP channels are implicated, underscores diversity in structural and regulatory features. Despite heavily conserved transmembrane domains, the cytoplasmic domains of TRP channels are notably different, which are the target of different gating and regulatory mechanisms (34, 35). Functional diversity by TRP family members also lies in the ability to hetero-oligomerize, thus creating a wider spectrum of TRP channel phenotypes. Although expected to be tetrameric structures, structural-functional evidence is only beginning to emerge (17). Moreover, the contribution of each monomeric unit to the functional channel complex is still largely unknown. In the present report, we demonstrated that PC2, TRPC1, and PC2/TRPC1 channel complexes are distinct units consistent with structural tetramers, which functionally correlate with the presence of subconductance states. This is in agreement with our original finding indicating that PC2 contains intrinsic subconductance states, whose resident times, can be modulated by changes in either cytoplasmic pH or holding potential (19). The presence of subconductance states has also been unmasked by functional inhibition with blocking agents such as amiloride, La^{3+}, and anti-PC2 antibodies (20). The question we posed in the present study was as to whether each one of the four subconductance states in PC2, has a structural correlation in its monomeric components.

The topology of PC2 and TRPC1 channels was assessed by AFM imaging of lipid bilayer imbedded complexes in solution, thus, providing the first direct comparison between structural and functional correlates of each channel complex. Although many channels are structural tetramers, the evidence for the putative tetrameric conformation of PC2, was heretofore, lacking. The correlation between the AFM imaging and the single channel currents indicates that each isolated monomer usually does not behave as a small conductance channel, but rather that at least four monomers of either protein (PC2 or TRPC1) are required to build a fully functional channel. The time residence and overall conductance at each substate are, therefore, a reflection of the number of contributing units to this tetrameric channel complex. The lack of evidence for isolated "monomeric" (small) channel conductances of PC2 in our preparations supports this contention. Full or partial PC2 channel inhibition by protonation at different pH suggests that in its fully closed state, the four channel subunits are protonated (19), which can then become sequentially functional, as each one changes conformation. This particular change in conformation is likely to be hindered in the presence of one or more TRPC1 subunits in the complex.

Distinct oligomerization, or “aggregation” domains (AD) (16) have been identified in the TRP superfamily members, including TRPC, TRPV, TRPM (please see (24, 40), for recent reviews) and even TRPP (PC2) (46). Both the carboxy and the amino termini domains of TRP channels have been implicated in these interactions (8, 10). These include the so-called TRP domain in the carboxy terminus (24), and the ankyrin domains found in the amino terminus region of several TRP channels. It is interesting to note, however, that neither one of these domains, is present in PC2. Original work by Tsiokas et al. (46), demonstrated that structural interactions between PC2 and TRPC1 also emanate from the transmembrane domains in PC2, which might be implicated in the aggregation of the hetero-complex (46). These putative association domains may also have functional correlates. Our findings

contend that specific aggregation regions in the monomers of the channel, once oligomerized into a functional complex, can be regulated by protonation, which plays both structural and functional roles by modifying the overall topological and conductive properties of the complex. Protonation in PC2, which we previously identified within the pore and is only reachable from the cytosolic side of the channel (19), likely helps screen charges and in turn allows conformational changes in the pore structure of the functional complex.

The tetrameric topology of PC2 and TRPC1 found in the current study is consistent with other channels, including the α_E subunit of the Ca^{2+} channel (31) and other TRP channels (1, 16, 23, 44). However, stoichiometries other than tetramer were also observed for PC2 with both AFM imaging and Western blot analysis. Similar findings have been reported in TRPV6 (23). FRET analysis of TRP channels further suggests a loosely packed tetramer (1), which may depend on the aggregation structure of the channel complex. Thus, although our data support a tetramer as the most plausible PC2 functional topology, they do not exclude other topological structures. In light of the present findings, the expectation is that the non-tetrameric TRP channel with either fewer or more interacting subunits, would display accordingly, different channel conductances and subconductance states. The ubiquitous distribution of TRP channels, including PC2 and TRPC1, and their ability to interact with each other (13, 46) may underlie their relevance and functional diversity in cell signaling. Our evidence indicates that the presence of at least one, most likely two TRPC1 monomers in the PC2/TRPC1 channel complex, elicits dramatic changes in the single channel conductance, open probability, and responses to pH and amiloride. This, in itself, indicates that the stoichiometric contribution of a particular channel has to be ascertained before any conclusions can be drawn, when assessing TRP-mediated whole-cell currents, or heterologous systems where more than one particular TRP channel is expected.

Our results are in agreement with recent literature, indicating that the isolated proteins have a somewhat similar behavior to cell expression systems. The single channel conductance of the tetrameric TRPC1 yielded a conductance of 22.8 pS, and a monomeric contribution of approximately 5 pS. This is slightly larger, but in agreement with recently reported data by Du et al (14), who showed that TRPC1 in glomerular mesangial cells has a single channel conductance of 17.2 pS. Bai et al (3), reported a TRPC1 conductance of 16 pS. It is important to note, however, that these were patch clamping studies in the biological membrane, where the channel complex may be affected by the associated proteins or structural lipids. Considering the technical and experimental differences, however, it can be accepted as in close agreement. Our data indicate that the interaction between TRPC1 and PC2 in a channel complex modifies the functional properties expected for each one alone. The single channel conductance of the PC2/TRPC1 hetero-complexes, was lower than PC2 homomers but higher than TRPC1 homomers, which is also in agreement with the results obtained by Bai et al. (3). Moreover, Bai et al. showed that TRPC1 was significantly activated by addition of the M1 muscarinic agonist oxotremorine-M (Oxo-M) in mIMCD3 cells, but was almost unresponsive to amiloride, a finding similar to ours for the isolated TRPC1 channel. They also demonstrated that co-transfection of PC2 with TRPC1 resulted in the formation of a channel with higher Ca^{2+} permeability, comparing to either channels alone, which confirms that TRPC1 and PC2 functionally interact to form an heteromultimer, resulting in the modulation of TRPC1 and PC2 properties. Our results , together with the published data, show the dramatic properties changes by heteromultimerization between PC2 and TRPC1.

AFM imaging of TRP (7) and other channels (4-6) has become recently available, which in combination with other high-resolution techniques such as cryo-electron microscopy (29, 30) has rendered nanometer resolution of a number of channels. For example, Sato's group recently provided evidence for a bell-shaped structure of TRPM2 (29) and TRPC3 (30); Barrera et al. have also observed the tetrameric structure of TRPC1 (7) and trimeric structure of P2X2 (6) using AFM imaging. In those studies, however, as in others from the same group (4, 5), the measurements, which are in strong agreement with their expected theoretical molecular volumes, are mostly consistent with a minimal volume occupied by the particles in solution. Because of the importance of membrane-channel interaction in determining the channel function, we studied the PC2/TRPC1 channel topology in lipid bilayers. The calculated molecular volumes of the PC2 or TRPC1 homomers in our study, suggest a much larger structures than their theoretical volumes, most likely the result of the conformational changes expected in the transmembrane structure of the channel protein in a lipid bilayer. When compared with more recent information on TRPC3 volume obtained from a molecular reconstruction of frozen hydrated samples by cryoelectron microscopy, for example, the value for TRPC3 is actually ten times larger than expected value from its molecular size. Using AFM, syncollin can be observed as a monomer of molecular volume similar to its theoretical value as a naked protein on mica (18). After insertion of the protein into lipid layers, syncollin shows a doughnut shape consistent with a hexamer. The molecular volume of these structures is, in average 706 nm^3, which would render a monomer of 118 nm^3, which is almost four times larger than the expected monomer (18). Recent AFM studies by Shahin et al (42) showed that the C2A and C2B domains of synaptotagmin, an integral membrane protein of the synaptic vesicle, dramatically changed in size when imbedded in lipid bilayers. They showed that C2AB has a calculated molecular volume of 80 nm^3, which is in agreement with the AFM measurement of 103 nm^3 under "naked" conditions. In lipid bilayers, however, much larger complexes of C2AB were observed. This report, which entails oligomerization (42), also shows that no particles in the 80 nm^3 range are observed, suggesting that even the monomers are likely larger in the membrane. Thus the calculated molecular volume of channels in lipids is generally larger than the expected theoretical value or without lipids. Conversely, it is also possible that channel insertion to the membrane also alters the lipid topological features and renders extrusions of membrane. Thus, the imaged channel structure in our AFM studies could include topological features from both channel proteins, and surrounding lipid bilayers. Our calculated channel diameters were much larger than those derived from solution without lipids. Therefore, it is important to begin assessing the contribution of the natural environment, i.e. the lipid bilayer, to the conformational topology of transmembrane proteins such as ion channels. This information is extremely relevant but has only recently begun to emerge. Previous studies from our laboratory (11) indicated that membrane imbedded CFTR has a molecular volume larger than its theoretical one. Interestingly, the calculated volume of PC2 is much larger than that of the homomeric TRPC1. This suggests a larger intramolecular space in PC2 as compared to TRPC1, which may help explain the larger pore conductance for PC2 (2) with respect to TRPC1. This phenomenon, which affects the electrophysiological and regulatory properties of the PC2/TRPC1 heteromeric complex, may also be reflected in the topological structure of the hetero-complex.

In summary, the data in this report indicate that both wild type PC2 and TRPC1 form homotetramers, with distinct functional and regulatory properties, among which there are the presence of four subconductance states in PC2. The AFM imaging of either of the respective homomers or the PC2/TRPC1 (2:2) hetero-complex is also consistent with a structural

tetramer. This structural interaction is reflected in a functional correlation, namely the PC2/TRPC1 heteromers have functional properties, which are distinct from either homomeric structure alone. The AFM imaging also makes evident that the lipid bilayer plays an important role in the topological features of these channel proteins, and supports the contention that structural features in solution of transmembrane proteins are suitably explored in their natural environment. Functional diversity among TRP channels, and in particular the channel properties of PC2 and TRPC1 indeed depends on their mutual interactions, which affect both channels. This type of structural-functional correlation of heterologous oligomerization may be the basis of functional diversity among the TRP family members, and extend to other members, and thus other functions associated with these cellular sensors.

Materials and Methods

Channel protein purification. PC2 protein was purified from HEK293T-S-PC2 cells overexpressing 6xHis-tagged PC2 protein. Ni-NTA spin columns (Qiagen, CA) and a protocol for protein purification under native conditions were conducted as per manufacturer's recommendations. Briefly, cells were suspended and homogenized in lysis buffer, containing 50 mM NaH_2PO_4, 300 mM NaCl, 1% NP-40, 10 mM imidazole, supplemented with pepstatin, aprotinin, leupeptin and PMSF, pH 8.0. After centrifugation of cell lysate at 10,000*g* for 30 min, the supernatant was applied to a lysis buffer pre-equilibrated Ni-NTA column. After centrifugation at 700*g* for 2 min, the column was twice washed with wash buffer 1, containing 50 mM NaH_2PO_4, 300 mM NaCl, 1% NP-40, 30 mM imidazole, and pepstatin, aprotinin, leupeptin and PMSF freshly, pH 8.0. This was followed by another two washes with wash buffer 2, containing 50 mM NaH_2PO_4, 300 mM NaCl, 2% NP-40, 25% glycerol, add pepstatin, aprotinin, leupeptin and PMSF, pH 8.0. PC2 was eluted from the column twice with elution buffer (50 mM NaH_2PO_4, 300 mM NaCl, 1% NP-40, 250 mM imidazole, and pepstatin, aprotinin, leupeptin and PMSF freshly, pH 8.0). TRPC1 preparation by flag affinity purification was conducted as follows. The purified flag-tagged protein was prepared from 293-S-TRPC1 cell lysates. Frozen cell pellets were added 1 ml Cellytic M reagent (Sigma), thawed out for 5min, and mixed well. The preparation was transferred to a 15-ml tube containing 4 ml Cellytic M reagent, and shake for another 15 min. The mixture was centrifuged and the supernatant of the cell lysate was loaded to the equilibrated column, and let flow through by gravity. The flow-through was collected, and the column was further washed with 5 ml (x1) of wash buffer. Proteins were eluted with 0.25 ml (x3) Flag peptide solution (200 ng/μl).

Western blot analysis of PC2. Western blot analyses were used to determine the size of the purified PC2 under both denaturing (SDS) and native conditions. Purified PC2 was electrophoresed in native- and SDS-PAGE, and followed by electro-transfer to enhanced chemiluminescence (ECL) nitrocellulose membranes. PC2 was blotted using either a polyclonal anti-PC2 antibody (#96525, 1:000 dilution) raised in rabbit to 44-62 amino acids of mouse PC2 intracellular N-terminal domain (12, 25, 27), or rabbit anti-polycystin-2 (Catalog #52-5217, 0.2 mg/ml Zymed, South San Francisco, CA). Immunoblotting was detected with ECL system.

Proteoliposome preparation. PC2-containing proteoliposomes were prepared with a 7:3 mixture of L-α-phosphatidylcholine (PC, 10 mg/ml, Avanti Polar Lipids, Inc., AL) and 1.2 ml of 1-palmitoyl-2-oleoyl-Sn-Glycero-3-phosphoethanolamine (PE, 25 mg/ml, Avanti) to get 40 mg lipid mixture in n-decane, which were dried with nitrogen. The lipid mixture was added 4 ml of Na^+-cholate buffer (25 mM Na^+-cholate, 150 mM NaCl, 0.1 mM EDTA, 20 mM HEPES, pH 7.2) and sonicated in a water bath sonicator for 45 min. To prepare PC2 containing proteoliposomes, purified PC2 (1 μg/μl) was diluted to 1:1000. Diluted PC2 (1 μl) was added to 100 μl of lipid solution described above, mixed well with 0.2 μl of Na^+-cholate and dialyzed against dialysis buffer (150 mM NaCl, 0.1 mM EDTA, 20 mM HEPES, pH 7.2) for 3 days at 4 ^oC (with three changes of buffer). Similar procedures were followed for TRPC1 proteoliposome preparation. For the preparation of TRPC1/PC2 channel complexes, the ratio between PC2 and TRPC1 in the previous prep was 1:1.

Ion channel reconstitution. Lipid bilayers were formed with a mixture of synthetic phospholipids (Avanti Polar Lipids, Birmingham, AL) in n-decane as reported (20). The lipid

mixture was made of 1-palmitoyl-2-oleoyl phosphatydil-choline and phosphatydil-ethanolamine in a 7:3 ratio. The lipid solution (~20-25 mg/ml) was spread over the aperture of a polystyrene cuvette (CP13-150) of a bilayer chamber (model BCH-13, Warner Instruments Corp.). Both sides of the lipid bilayer were bathed with a solution containing MOPS-KOH, 10 mM, and MES-KOH, 10 mM, pH 7.40, and 10-15 μM Ca^{2+}. Both sides of the chamber had an initial, 15 mM K^+ concentration, which was further supplemented to 150 mM in the *cis* side of the chamber to create a chemical gradient. Either membrane vesicles or proteoliposomes were added, to the *cis* side of the chamber. Wherever indicated, PC2 channel activity was determined from enriched human syncytiotrophoblast membranes as reported (20).

Electrophysiological data acquisition and analysis. Electrical signals were recorded with a PC-501A patch clamp amplifier (Warner Instruments. Corp.), using a 10 Gohm feedback resistor. Output signals were low-pass filtered at 1 kHz. Signals were displayed on an oscilloscope, and channel recordings were stored in a personal computer. Single channel current tracings were further filtered for display purposes only. Unless otherwise stated, either pCLAMP Versions 5.5.1 or 10.0 (Axon Instruments, Foster City, CA) were used for data analysis. Sigmaplot Version 2.0 (Jandel Scientific, Corte Madera, CA) was used for statistical analysis and graphics. Single channel conductances were calculated as reported (19, 20). Statistical significance was obtained by unpaired Student's "t" test comparison of sample groups of similar size. Average data values were expressed as the mean ± SEM (n) under each condition, where n represents the total number of experiments analyzed. Statistical significance was accepted at $p<0.05$.

Atomic force microscopy. PC2 and TRPC1 channel complexes were imaged with either a Model 3000 atomic force microscope (AFM) attached to a Nanoscope IIIa controller (Veeco Metrology, St. Barbara, CA) as reported (11, 38), or a Model 3100 AFM attached to a NanoScope V controller, a kind loan from Veeco Metrology (see Acknowledgments). Samples were scanned with oxide-sharpened silicon-nitride tips (DNP-S, Veeco Metrology). Channel-containing proteoliposomes used for the lipid-bilayer reconstitution studies were used for AFM imaging studies. Proteoliposomes suspended in saline solution, containing 0.2 mM $CaCl_2$, 0.2 mM MgATP, 0.2 mM β-mercaptoethanol and 2 mM Tris-HCl, pH 7.15-7.25 were placed onto freshly cleaved mica disks. Proteoliposomes were flattened onto the mica surface by incubation for ~30 min at 37 ^oC. Changes in saline pH were conducted by addition of HCl (1.0 N) to the solution in the scanning chamber.

Determination of molecular dimensions. The calculation of molecular dimensions for the various channel complexes was followed as originally reported by Schneider et al (41). Briefly, multiple cross-sections of individual protein images by AFM were made and the mean diameters and heights of each unit were measured. As previously reported, we measured the diameter at half-maximal height of individual molecules, which sufficiently compensates for the artificially induced overestimation of the protein width. The molecular volume was calculated, after obtaining the dimensions of an individual protein (diameter and height), by treating the protein as a segment of a sphere. This calculation was done with the following equation, $V_m = (\pi h/6)\,(3r^2 + h^2)$, where V_m is the molecular volume, and h and r are the height and the radius of the protein, respectively. In addition, the molecular volume of the protein was calculated using the following equation: $V_c = (M_o/N_o)(V_1 + dV_2)$. Here, M_o is the molecular weight, N_o is Avogadro's number, and V_1 and V_2 are the partial specific volumes of

the individual protein (0.74 cm^3g^{-1}, and 1 cm^3g^{-1} water, respectively). *d* is the extent of protein hydration (0.4 mol H_2O/mol protein) (41).

Acknowledgements

The authors (HFC and JZ) wish to acknowledge the PKD Foundation for support of these studies. WHG present address: Center for Medical Physics and Technology, Friedrich Alexander University, Erlangen-Nuerenberg, Germany. HFC and his group wish to thank Dean Schmidt, Kim Reed, and John Thornton from Veeco Metrology (Sta. Barbara, CA) for lending the Dimension 3100 atomic force microscope coupled to the NanoScope V controller, with which AFM imaging was made possible.

Conflict of Interest Statement
None declared.

References

1. Amiri, H., G. Schultz, and M. Schaefer. (2003) FRET-based analysis of TRPC subunit stoichiometry. *Cell Calcium* **33**, 463-470.
2. Anyatonwu, G. I., and B. E. Ehrlich. (2005) Organic cation permeation through the channel formed by polycystin-2. *J. Biol. Chem.* **280**, 29488-29493.
3. Bai, C.-X., A. Giamarchi, L. Rodat-Despoix, F. Padilla, T. Downs, L. Tsiokas, and P. Delmas. (2008) Formation of a new receptor-operated channel by heteromeric assembly of TRPP2 and TRPC1 subunits. *EMBO reports* **9**, 472-479.
4. Barrera, N. P., R. M. Henderson, and J. M. Edwardson. (2008) Determination of the architecture of ionotropic receptors using AFM imaging. Invited Review. *Pflügers Arch. - Eur. J. Physiol.* **456**, 199-209.
5. Barrera, N. P., P. Herbert, R. M. Henderson, I. L. Martin, and J. M. Edwardson. (2005) Atomic force microscopy reveals the stoichiometry and subunit arrangement of 5-HT3 receptors. *Proc. Natl. Acad. Sci. USA* **102**, 12595–12600.
6. Barrera, N. P., S. J. Ormond, R. M. Henderson, R. D. Murrell-Lagnado, and J. M. Edwardson. (2005) Atomic force microscopy imaging demonstrates that P2X2 receptors are trimers but that P2X6 receptor subunits do not oligomerize. *J. Biol. Chem.* **280**, 10759-10765.
7. Barrera, N. P., Y. Shaifa, I. McFadzean, J. T. P. Ward, R. M. Henderson, and J. M. Edwardson. (2007) AFM imaging reveals the tetrameric structure of the TRPC1 channel. *Biochem. Biophys. Res. Comm.* **358**, 1086-1090.
8. Becker, D., M. Müller, K. Leuner, and M. Jendrach. (2008) The C-terminal domain of TRPV4 is essential for plasma membrane localization. *Mol. Membr. Biol.* **25**, 139-151.
9. Catterall, W. A. (2000) Structure and regulation of voltage-gated Ca^{2+} channels. *Annu. Rev. Cell Dev. Biol.* **16**, 521-555.
10. Celic, A., E. T. Petri, B. Demeler, B. E. Ehrlich, and T. J. Boggon. (2008) Domain mapping of the polycystin-2 C-terminal tail using de novo molecular modeling and biophysical analysis. *J. Biol. Chem.* **283**, 28305-28312.
11. Chasan, B., N. A. Geisse, K. Pedatella, D. G. Wooster, M. Teintze, M. D. Carattino, W. H. Goldmann, and H. F. Cantiello. (2002) Evidence for direct interaction between actin and the cystic fibrosis transmembrane conductance regulator. *Eur. Biophys. J.* **30**, 617-624.
12. Dedoussis, G. V. Z., Y. Luo, P. Starremans, S. Rossetti, A. J. Ramos, H. F. Cantiello, E. Katsareli, P. Ziroyannis, K. Lamnissou, P. C. Harris, and J. Zhou. (2008) Co-inheritance of a PKD1 mutation and homozygous PKD2 variant: a potential modifier in autosomal dominant polycystic kidney disease. *Eur. J. Clin. Invest.* **38**, 180-190.
13. Delmas, P. (2004) Assembly and gating of TRPC channels in signalling microdomains. *Novartis Found. Symp.* **258**, 75-97.
14. Du, J., S. Sours-Brothers, R. Coleman, M. Ding, S. Graham, D.-H. Kong, and R. Ma. (2007) Canonical transient receptor potential 1 channel is involved in contractile function of glomerular mesangial cells. *J Am Soc Nephrol* **18**, 1437-1445.
15. Ferrer-Montiel, A., C. García-Martinez, C. Morenilla-Palao, N. García-Sanz, A. Fernandez-Carvajal, G. Fernandez-Ballester, and R. Planells-Cases. (2004) Molecular architecture of the vanilloid receptor. Insights for drug design. *Eur. J. Biochem.* **271**, 1820-1826.
16. García-Sanz, N., A. Fernandez-Carvajal, C. Morenilla-Palao, R. Planells-Cases, E. Fajardo-Sanchez, G. Fernandez-Ballester, and A. Ferrer-Montiel. (2004)

Identification of a tetramerization domain in the C terminus of the vanilloid receptor. *J. Neurosci.* **24**, 5307-5314.

17. Gaudet, R. (2008) TRP channels entering the structural era. *J. Physiol.* **586**, 3565-3575.
18. Geisse, N. A., B. Wäsle, D. E. Saslowsky, R. M. Henderson, and J. M. Edardson. (2002) Syncollin homo-oligomers associate with lipid bilayers in the form of doughnut-shaped structures. *J. Membr. Biol.* **189**, 83-92.
19. González-Perrett, S., M. Batelli, K. Kim, M. Essafi, G. Timpanaro, N. Montalbetti, I. L. Reisin, M. A. Arnaout, and H. F. Cantiello. (2002) Voltage dependence and pH regulation of human polycystin-2 mediated cation channel activity. *J. Biol. Chem.* **277**, 24959-24966.
20. González-Perrett, S., K. Kim, C. Ibarra, A. E. Damiano, E. Zotta, M. Batelli, P. C. Harris, I. L. Reisin, M. A. Arnaout, and H. F. Cantiello. (2001) Polycystin-2, the protein mutated in autosomal dominant polycystic kidney disease (ADPKD), is a Ca^{2+}-permeable nonselective cation channel. *Proc. Ntal. Acad. Sci. USA* **98**, 1182-1187.
21. Hoenderop, J. G., T. Voets, S. Hoefs, F. Weidema, J. Prenen, B. Nilius, and R. J. Bindels. (2003) Homo- and heterotetrameric architecture of the epithelial Ca^{2+} channels TRPV5 and TRPV6. *EMBO J.* **22**, 776-785.
22. Johnson Jr., J. P., and W. N. Zagotta. (2001) Rotational movement during cyclic nucleotide-gated channel opening. *Nature* **412**, 917-921.
23. Kedei, N., T. Szabo, J. D. Lile, J. J. Treanor, Z. Olah, M. J. Iadarola, and P. M. Blumberg. (2001) Analysis of the native quaternary structure of vanilloid receptor 1. *J. Biol. Chem.* **276**, 28613-28619.
24. Lepage, P. K., and G. Boulay. (2007) Molecular determinants of TRP channel assembly. *Biochem. Soc. TRansact.* **35**, 81-83.
25. Li, Q., N. Montalbetti, P. Y. Shen, X.-Q. Dai, C. I. Cheeseman, E. Karpinski, G. Wu, H. F. Cantiello, and X.-Z. Chen. (2005) Alpha-actinin associates with polycystin-2 and regulates its channel activity. *Hum. Mol. Genet.* **14**, 1587-1603.
26. Liu, D. T., S. A. Tibbs, and S. A. Siegelbaum. (1996) Subunit stoichiometry of cyclic nucleotide-gated channesl and effects of subunit order on channel function. *Neuron* **16**, 983-990.
27. Luo, Y., P. M. Vassilev, X. Li, Y. Kawanabe, and J. Zhou. (2003) Native polycystin 2 functions as a plasma membrane Ca^{2+}-permeable cation channel in renal epithelia. *Mol. Cell. Biol.* **23**, 2600-2607.
28. MacKinnon, R. (1991) Determination of the subunit stoichiometry of a voltage-activated potassium channel. *Nature* **350**, 232-235.
29. Maruyama, Y., T. Ogura, K. Mio, S. Kiyonaka, K. Kato, Y. Mori, and C. Sato. (2007) Three-dimensional reconstruction using transmission electron microscopy reveals a swollen, bell-shaped structure of transient receptor potential melastatin type 2 cation channel. *J. Biol. Chem.* **282**, 36961-36970.
30. Mio, K., T. Ogura, Y. Hara, Y. Mori, and C. Sato. (2005) The non-selective cation-permeable channel TRPC3 is a tetrahedron with a cap on the large cytoplasmic end. *Biochem. Biophys. Res. Commun.* **333**, 768-777.
31. Mochizuki, T., G. Wu, T. Hayashi, S. L. Xenophontos, B. Veldhuisen, J. J. Saris, D. M. Reynolds, Y. Cai, P. A. Gabow, A. Pierides, W. J. Kimberling, M. H. Breuning, C. C. Deltas, D. J. Peters, and S. Somlo. (1996) PKD2, a gene for polycystic kidney disease that encodes an integral membrane protein. *Science* **272**, 1339-1342.

32. Montalbetti, N., Q. Li, G. A. Timpanaro, S. González-Perrett, X.-Q. Dai, X.-Z. Chen, and H. F. Cantiello. (2005) Cytoskeletal regulation of calcium-permeable cation channels in the human syncytiotrophoblast. Role of gelsolin. *J. Physiol. (London)* **566**, 309-325.
33. Montalbetti, N., Q. Li, Y. Wu, X.-Z. Chen, and H. F. Cantiello. (2007) Polycystin-2 cation channel function in the human syncytiotrophoblast is regulated by microtubular structures. *J. Physiol.* **579**, 717-728.
34. Montell, C. (2001) Physiology, phylogeny, and functions of the TRP superfamily of cation channels. *Sci. STKE* **90**, RE1.
35. Montell, C., L. Birnbaumer, and V. Flockerzi. (2002) The TRP channels, a remarkably functional family. *Cell* **108**, 595-598.
36. Montell, C., L. Birnbaumer, V. Flockerzi, R. J. Bindels, E. A. Bruford, M. J. Caterina, D. E. Clapham, C. Harteneck, S. Heller, D. Julius, I. Kojima, Y. Mori, R. Penner, D. Prawitt, A. M. Scharenberg, G. Schultz, N. Shimizu, and M. X. Zhu. (2002) A unified nomenclature for the superfamily of TRP cation channels. *Mol. Cell* **9**, 229-231.
37. Nauli, S. M., F. J. Alenghat, Y. Luo, E. Williams, P. Vassilev, X. Li, A. E. H. Elia, W. Lu, E. M. Brown, S. J. Quinn, D. E. Ingber, and J. Zhou. (2003) Polycystins 1 and 2 mediate mechanosensation in the primary cilium of kidney cells. *Nature Genet* **. 33**, 129-137.
38. Raychowdhury, M. K., S. González-Perrett, N. Montalbetti, G. A. Timpanaro, B. Chasan, W. H. Goldmann, S. Stahl, A. Cooney, E. Goldin, and H. F. Cantiello. (2004) Molecular pathophysiology of mucolipidosis type IV. pH dysregulation of the human mucolipin-1 cation channel. *Hum. Mol. Genet.* **13**, 617-627.
39. Rosenmund, C., Y. Stern-Bach, and C. F. Stevens. (1998) The tetrameric structure of a glutamate receptor channel. *Science* **280**, 1596-1599.
40. Schindl, R., and C. Romanin. (2007) Assembly domains in TRP channels. *Biochem. Soc. Transact.* **35**, 84-85.
41. Schneider, S. W., J. Lärmer, R. M. Henderson, and H. Oberleithner. (1998) Molecular weights of individual proteins correlate with molecular volumes measured by atomic force microscopy. *Pflügers Arch.* **435**, 362-367.
42. Shahin, V., D. Datta, E. Hui, R. M. Henderson, E. R. Chapman, and J. M. Edwardson. (2008) Synaptotagmin perturbs the structure of phospholipid bilayers. *Biochemistry* **47**, 2134-2152.
43. Strübing, C., G. Krapivinsky, L. Krapivinsky, and D. E. Clapham. (2003) Formation of novel TRPC channels by complex subunit interactions in embryonic brain. *J. Biol. Chem.* **278**, 39014-39019.
44. Szallasi, A., and P. M. Blumberg. (1991) Molecular target size of the vanilloid (capsaicin) receptor in pig dorsal root ganglia. *Life Sci.* **48**, 1863-1869.
45. Torres, V. E., Y. Cai, X. Chen, G. Q. Wu, L. Geng, K. A. Cleghom, C. M. Johnson, and S. Somlo. (2001) Vascular expression of polycystin-2. *J. Am. Soc. Nephrol.* **12**, 1-9.
46. Tsiokas, L., T. Arnould, C. Zhu, E. Kim, G. Walz, and V. P. Sukhatme. (1999) Specific association of the gene product of PKD2 with the TRPC1 channel. *Proc. Natl. Acad. Sci. USA* **96**, 3934-3939.
47. Vassilev, P. M., L. Guo, X. Z. Chen, Y. Segal, J. B. Peng, N. Basora, H. Babakhanlou, G. Cruger, M. Kanazirska, C. Ye, E. M. Brown, M. A. Hediger, and J. Zhou. (2001) Polycystin-2 is a novel cation channel implicated in defective intracellular Ca^{2+} homeostasis in polycystic kidney disease. *Biochem. Biophys. Res. Commun.* **282**, 341-350.

48. Wu, Y., X.-Q. Dai, Q. Li, C. X. Chen, S. Cho, Z. Hussain, N. Montalbetti, G. Li, R. Glynne, S. Wang, H. F. Cantiello, G. Wu, and X.-Z. Chen. (2006) Kinesin-2 mediates physical and functional interactions between polycystin-2 and fibrocystin. *Hum. Mol. Genet.* **15**, 3280-3292.
49. Xu, X. Z., H. S. Li, W. B. Guggino, and C. Montell. (1997) Coassembly of TRP and TRPL produces a distinct store-operated conductance. *Cell* **89**, 1155-1164.

Legends to Figures

Fig. 1: *Presence of subconductance states in the PC2 channel.* (**a**) Single channel currents of endogenous hST PC2. Holding potential is 60 mV in asymmetrical K^+. (**b**) Three intermediate subconductance levels are identifiable in the all-point histogram. C, closing state; O_1-O_4, 4 sub-conductance states. **(c)** Expanded single channel current subconductance states of PC2 from region indicated with horizontal line in (**a**). (**d**) Examples of subconductance states in the purified PC2 reconstituted protein as in (19). Spontaneous, full channel closures (arrow), are followed by "staircase" activation of the four subconductance states, revealing four identical functional subunits (dashed lines). This is further evidenced by the mean *vs.* variance analysis of the tracing (Right). (**e**) The mean activation was calculated by averaging kinetics after full closures. Voltage-dependence of subconductance states (open circles, 40 mV, compared to filled symbols, 0 mV, $p<0.02$). Data are the average of nine and seven sojourns, from five experiments, respectively. Averages do not display discrete steps, indicating the variable time spent by the channel at each subconductance level. There is a kinetic delay only observed at 0 mV. (**f**) Spontaneous subconductance states in PC2 (Top, dashed lines) can be further modified by reduction in cytoplasmic pH (*cis* chamber), which decreases PC2 channel activity as previously reported (19). Solid lines indicate the respective averages at normal pH (7.25, also see Fig. 1d). (**g**) The quaternary structure of PC2 was confirmed by gel electrophoresis of affinity purified PC2 under denaturing (Left) and non-denaturing (Right) conditions. The presence of 440 kDa protein complexes (tetramers) were observed under non-denaturing conditions, in contrast to denaturing conditions, which only showed monomers (~110 kDa), dimers (~210 kDa) and a cleaved form of PC2 (~70 kDa). Lane 1 indicates purified protein and Lane 2 the whole cell lysate in the native gel (right).

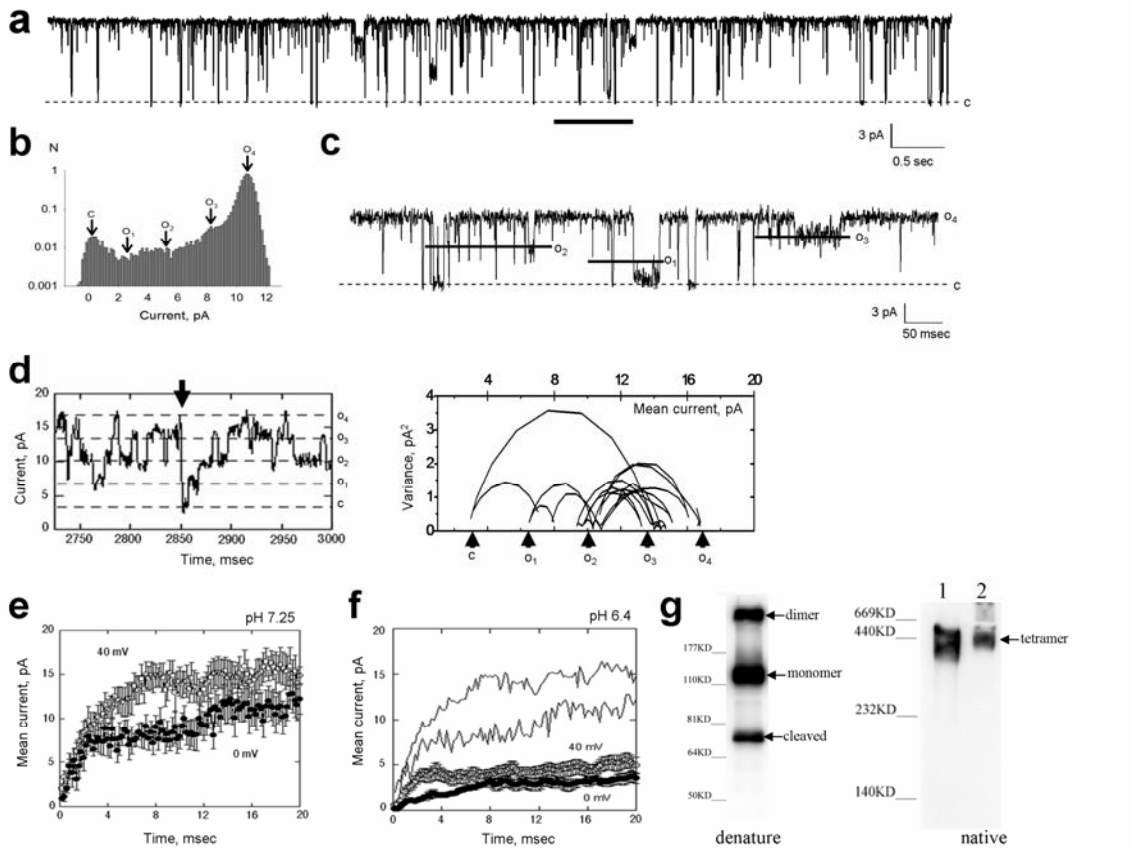
a
c
b
N
Current, pA
c
o1
o2
o3
o4
3 pA
0.5 sec
3 pA
50 msec
d
Current, pA
Time, msec
Variance, pA2
Mean current, pA
e
pH 7.25
40 mV
0 mV
Mean current, pA
Time, msec
f
pH 6.4
40 mV
0 mV
Mean current, pA
Time, msec
g
dimer
monomer
cleaved
177KD
110KD
81KD
64KD
50KD
denature
1
2
669KD
440KD
232KD
140KD
tetramer
native

Fig. 2: *Electrophysiology of the TRPC1 channel.* (**a**) Single channel currents of affinity purified TRPC1 at different holding potentials in asymmetrical K^+. (**b**) Current-to-voltage relationship for the TRPC1, indicating a single channel conductance of 5.0 ± 0.7 pS (n=5), and a bigger conductance of 22.8 ± 2.0 pS (n=5). (**c**) Representative tracing showing a TRPC1 channel complex display four subconductance states at +100 mV. (**d**) All-point histogram of (c) shows the presence of four subconductance states in TRPC1. (**e**). Effect of amiloride (200 μM, *trans* side) on TRPC1 single channel currents. Addition of amiloride to the *trans* chamber was without effect on the purified channel. Representative tracings from n=10. (**f**). Lowering the cytoplasmic pH had no effect on the TRPC1 single channel currents. The cytoplasmic pH was reduced by addition of 1.0 N HCl to the *cis* chamber. Data representative of n=7 experiments.

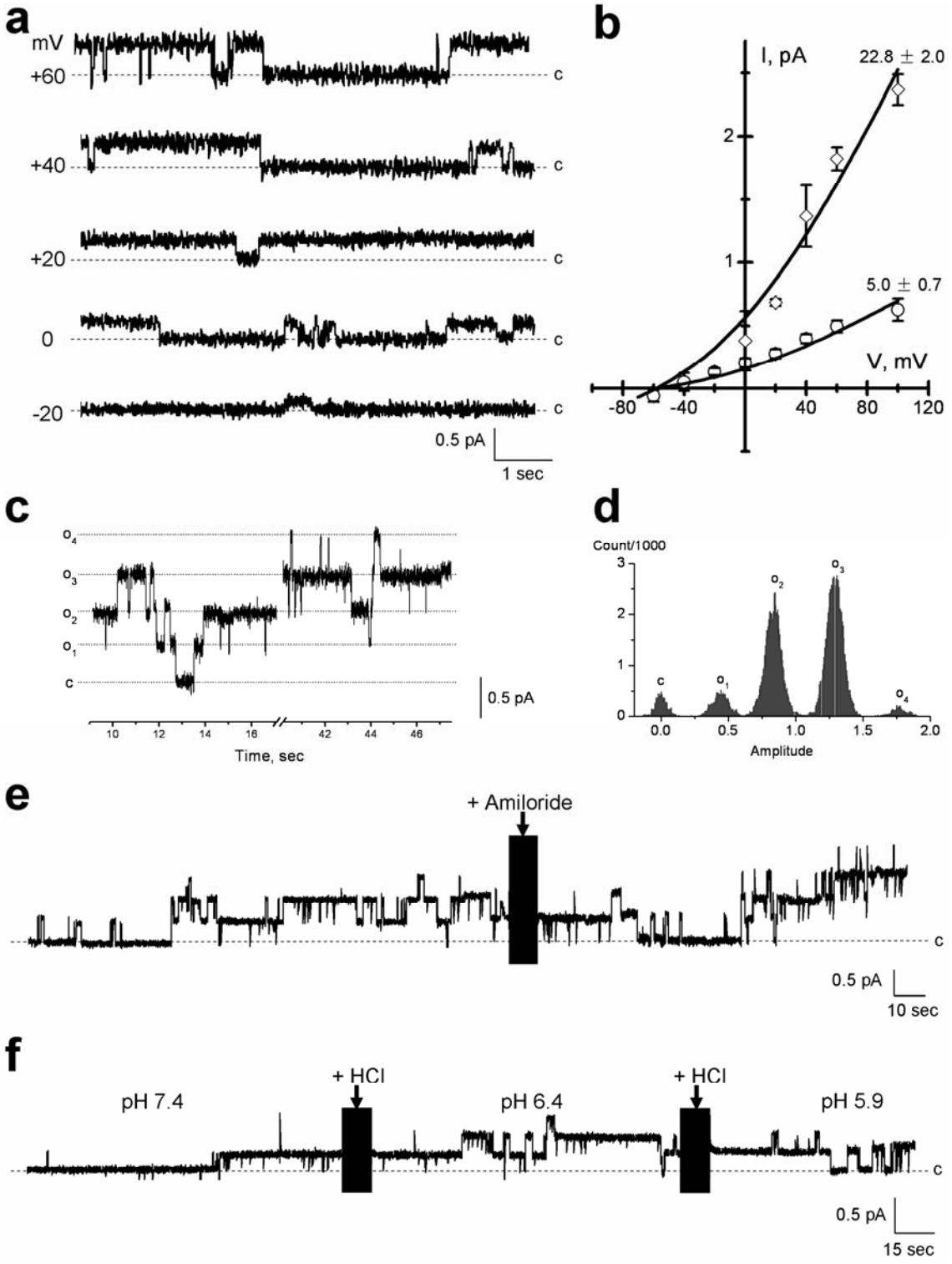
a
mV
+60
+40
+20
0
-20
c
0.5 pA
1 sec
b
I, pA
22.8 ± 2.0
5.0 ± 0.7
V, mV
-80
-40
40
80
120
1
2
c
o4
o3
o2
o1
c
0.5 pA
10
12
14
16
42
44
46
Time, sec
d
Count/1000
3
2
1
0
c
o1
o2
o3
o4
0.0
0.5
1.0
1.5
2.0
Amplitude
e
+ Amiloride
c
0.5 pA
10 sec
f
pH 7.4
+ HCl
pH 6.4
+ HCl
pH 5.9
c
0.5 pA
15 sec

Fig. 3: *Electrophysiological features of the PC2/TRPC1 hetero-complex.* PC2/TRPC1 hetero-complex displayed two conductances (**a, b**), which are corresponding to the smaller TRPC1 and bigger PC2 channels. (**c**) Shows the all point histogram of the extended tracing (b). (**d**) The I-V relationship of PC2/TRPC1 hetero-complex shows a conductance (red lines and circle) between those of homomeric PC2 (157 pS, higher grey dashed line) (19) and homomeric TRPC1 (~23 pS, lower green line indicates the fitted I-V relationship for TRPC1 homomers as shown in Fig. 2b). There is also a lower conductance present in the PC2/TRPC1 hetero-complexes (the blue triangles and line), which is close to the conductance of homomeric TRPC1. The black square represents PC2/TRPC1 complexes showing a higher conductance, closer to PC2 contribution alone. (**e**) The bar graph for the conductance of PC2, TRPC1 and PC2/TRPC1 complexes indicates that the single channel conductance of the heterocomplex is statistically different from either homomer alone. * indicates $p<0.001$.

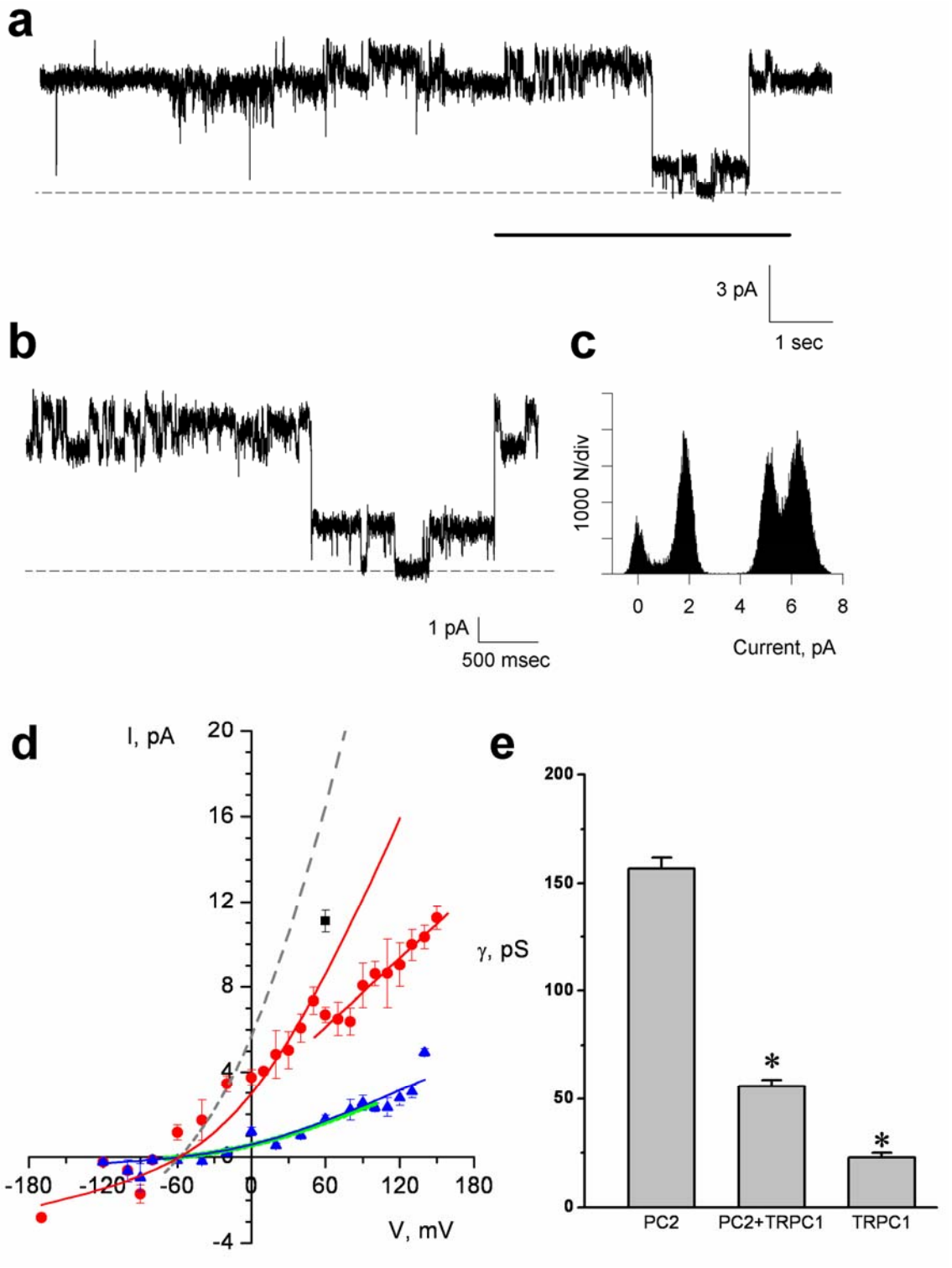
a
3 pA
1 sec
b
1 pA
500 msec
c
1000 N/div
0
2
4
6
8
Current, pA
d
I, pA
20
16
12
8
4
0
-4
-180
-120
-60
0
60
120
180
V, mV
e
γ, pS
200
150
100
50
0
*
*
PC2
PC2+TRPC1
TRPC1

Fig. 4: *Electrophysiological features of the PC2/TRPC1 hetero-complex. Effect of amiloride.* (**a**) Single channel currents of reconstituted PC2/TRPC1 channel complexes in asymmetrical K^+. Note the flickering in the large conductance deflections, consistent with PC2 contribution, contrasting the much longer open probability of the small conductance states observed in the TRPC1 channel contribution to the complex. (**b**) Expanded single channel currents unmask the large conductance PC2, and smaller conductance TRPC1 under control conditions. (**c**) PC2 conductance was blocked by amiloride but TRPC1 conductance persisted. All-point histograms to the right side of the panels indicate the channel conductances under each condition. Data are representative of n=7 independent experiments.

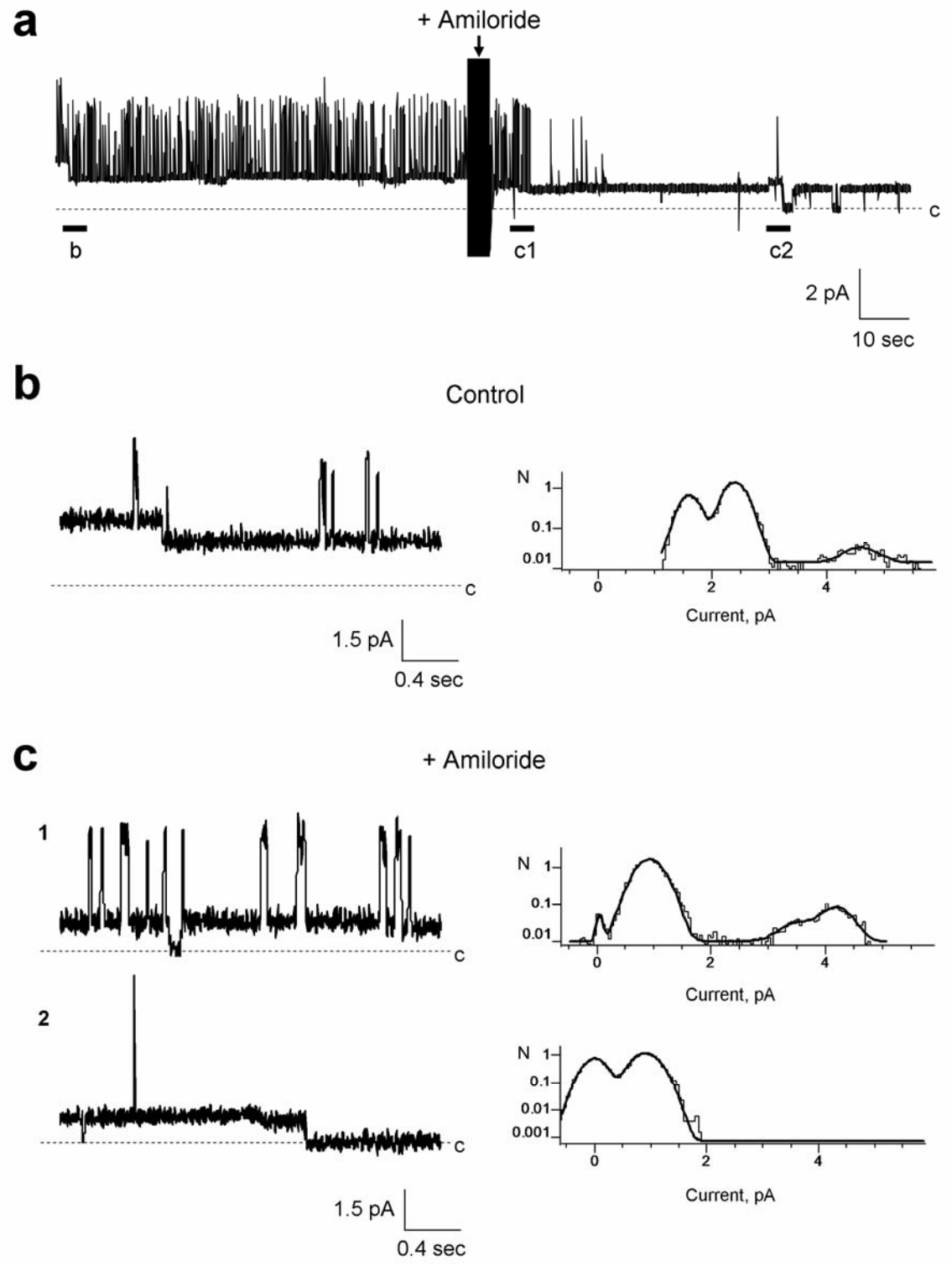
a
+ Amiloride
b
c1
c2
c
2 pA
10 sec
b
Control
c
1.5 pA
0.4 sec
N
1
0.1
0.01
0
2
4
Current, pA
c
+ Amiloride
1
2
c
1.5 pA
0.4 sec
N
1
0.1
0.01
0.001
0
2
4
Current, pA

Fig. 5: *Electrophysiological features of the PC2/TRPC1 hetero-complex. Effect of lowering pH.* The PC2/TRPC1 hetero-complexes were insensitive to changes in pH (*cis* chamber). Data were obtained in the presence of KCl chemical gradient. Lowering the pH to either 6.4 (**a**), or 5.9 (**b**) had no effect on the channel activity of PC2/TRPC1 hetero-complexes. Data are representative of n=7.

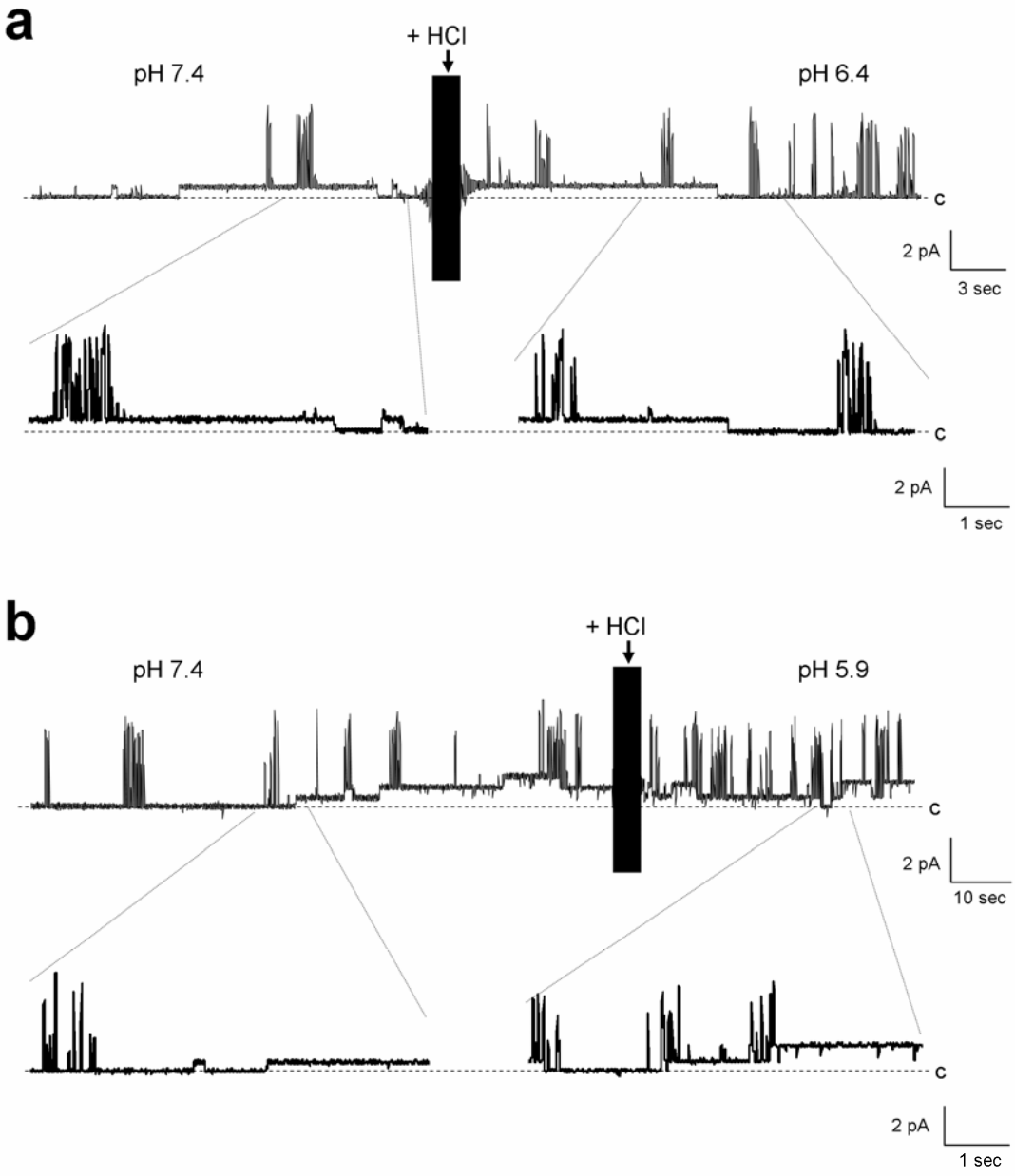
a
+ HCl
pH 7.4
pH 6.4
c
2 pA
3 sec
c
2 pA
1 sec
b
+ HCl
pH 7.4
pH 5.9
c
2 pA
10 sec
c
2 pA
1 sec

Fig. 6: *AFM imaging of PC2*. (**a**) PC2 was imaged in flattened, PC2-containing proteoliposomes, onto freshly cleaved mica in saline solution. (**b**) Upper panel, PC2 channels were identified in AFM scans as round structures, often displaying a central indentation, and a tetra-lobular structure. Lower panel (1-3) showed three expanded PC2 structure highlighted in the circle in the upper panel. (**c**) Cross section histograms from the b1-b3 indicate the height and diameter of the contributing monomers, and the central indentation. Three such measurements are superimposed in the graph. (**d**) Population analysis of channel units, indicate that the monomers segregated in a scattered population (n=107). (**e**) Analysis of the distribution of diameters indicates two peaks, suggesting asymmetry in the shape of the channels. (**f**) Further analysis of the distribution of heights indicates three peaks.

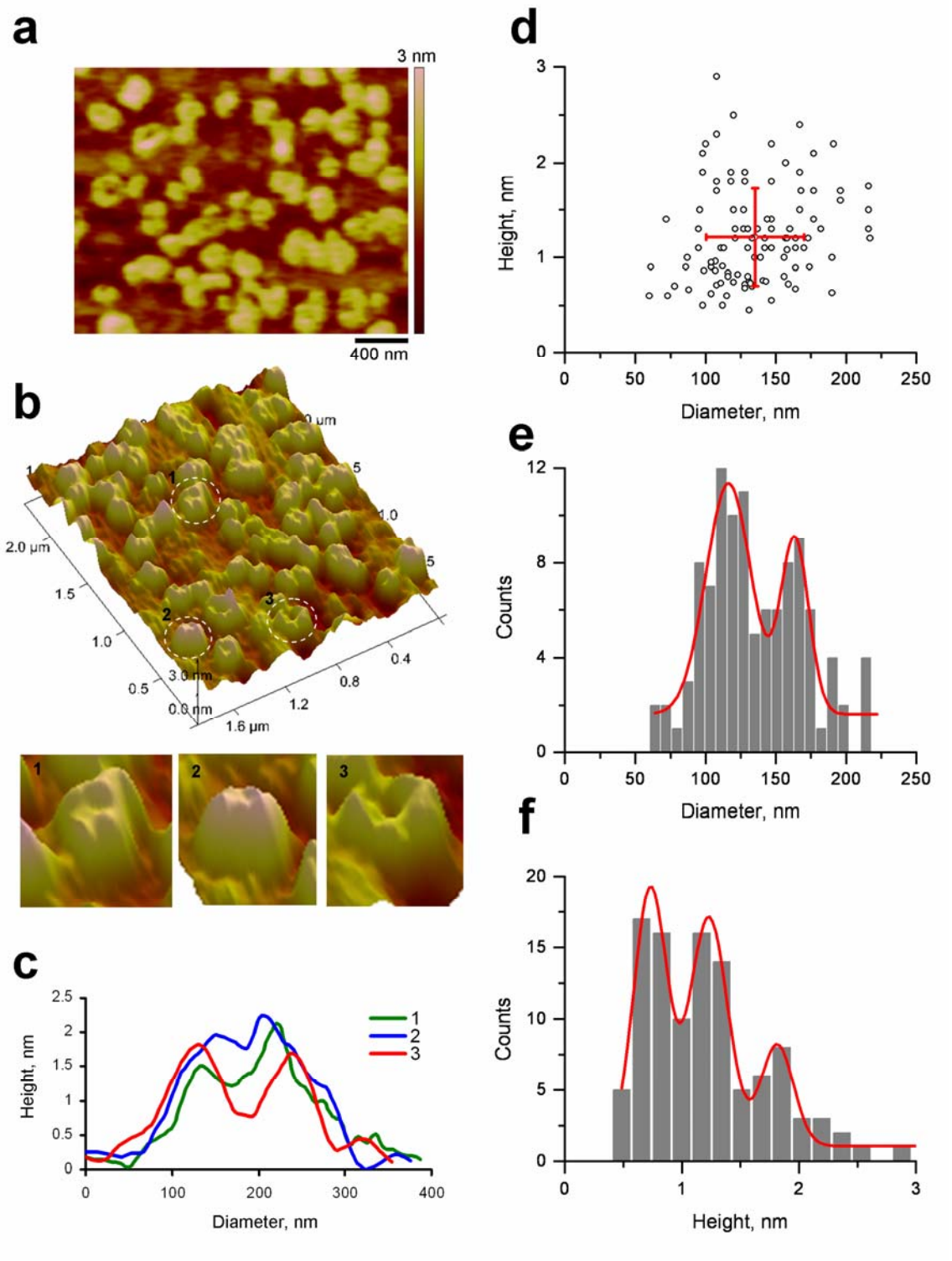
a
3 nm
400 nm
b
2.0 µm
1.5
1.0
0.5
0.0 nm
3.0 nm
0.4
0.8
1.2
1.6 µm
1
2
3
c
Height, nm
Diameter, nm
d
Height, nm
Diameter, nm
e
Counts
Diameter, nm
f
Counts
Height, nm

Fig. 7: *Effect of anti-PC2 antibody on AFM imaging of PC2.* (**a**) PC2 monomers were identified in AFM scans (Scale bar, 500 nm) as round structures and the exposure to the anti-PC2 antibody (Zymed Catalog # 52-5217) increased both the height and the diameter of PC2. (**b**) The cross sections at the lines indicated in (**a**), show the binding of PC2 antibody increased the apparent diameter and the height of PC2. Data are representative of two paired experiments.

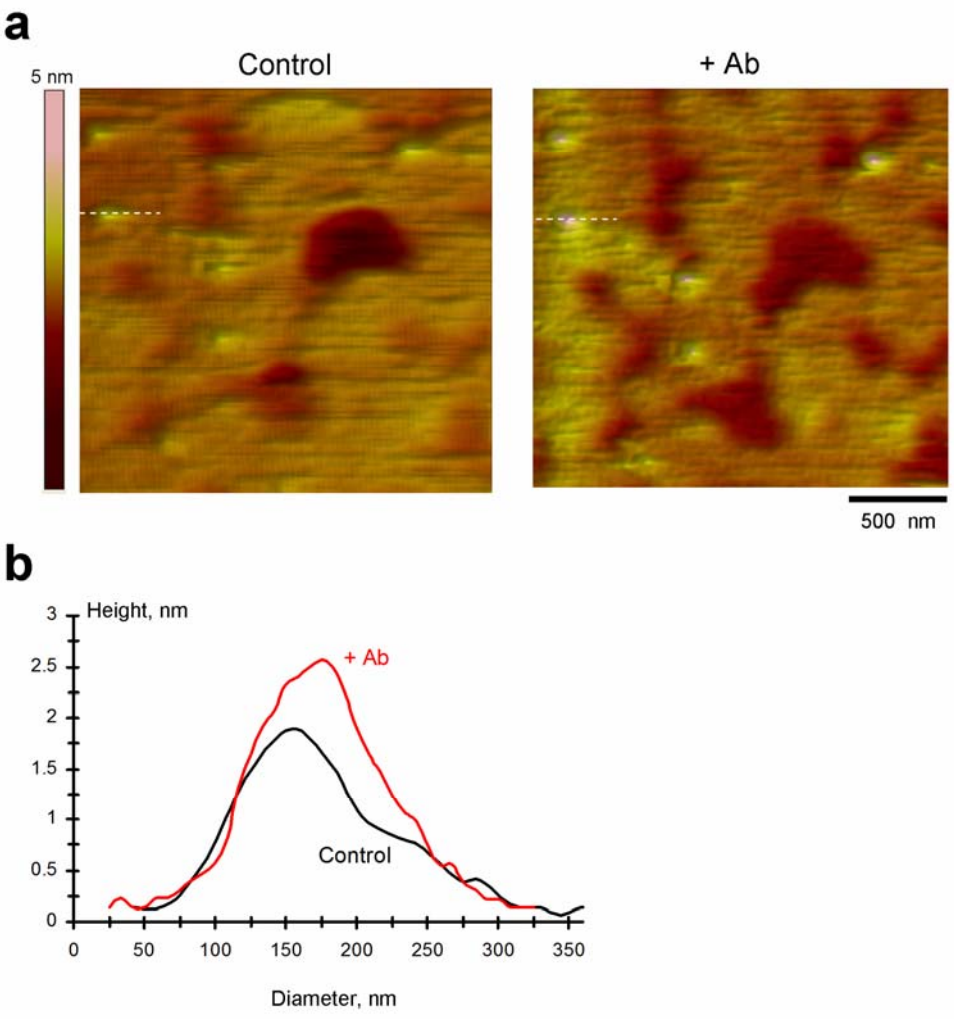
a
Control
+ Ab
5 nm
500 nm
b
Height, nm
+ Ab
Control
Diameter, nm
0
0.5
1
1.5
2
2.5
3
0
50
100
150
200
250
300
350

Fig. 8: *Changes in AFM imaging of PC2 at low pH.* (**a**) PC2 was imaged in flattened, PC2-containing proteoliposomes, onto freshly cleaved mica in saline solution (pH 7.4). (**b**) Lowering the sample's pH (~6.1) decreased PC2's extra-membrane size. Data are representative of three paired experiments.

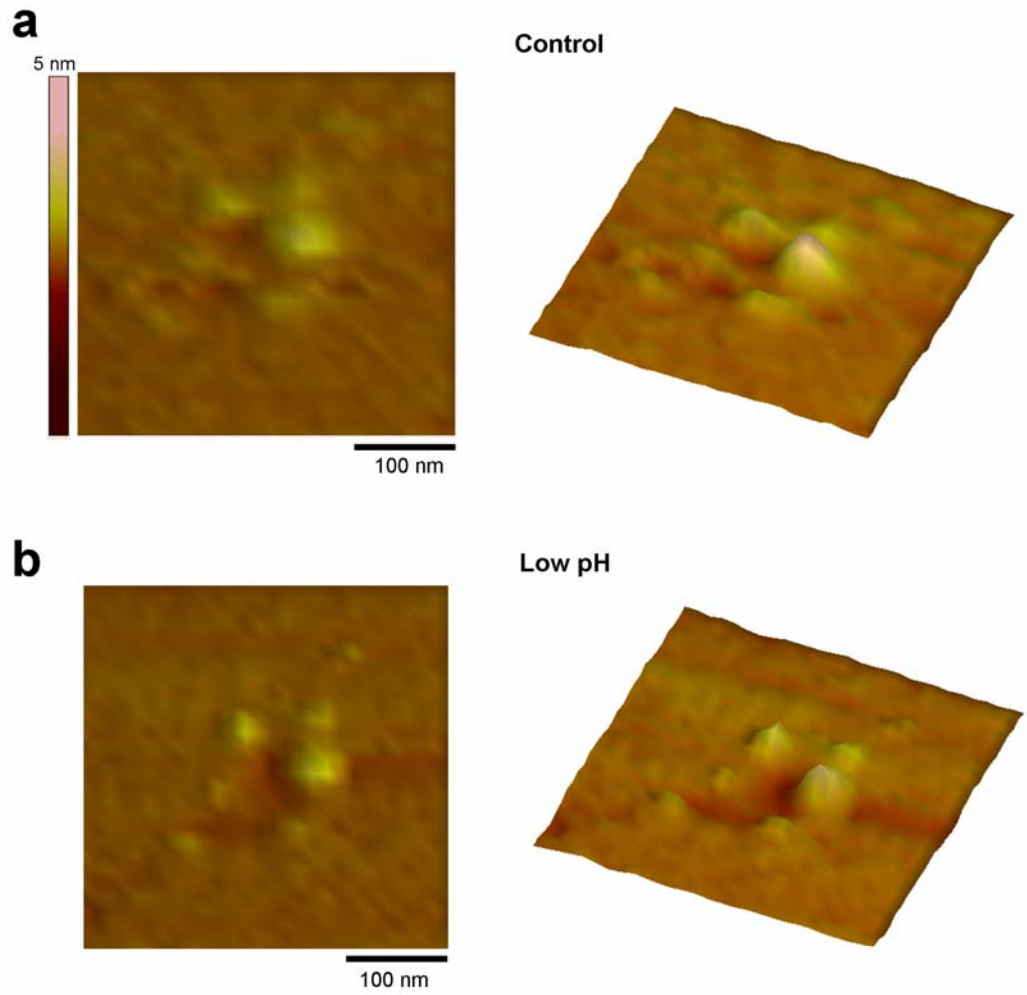
a
5 nm
100 nm
Control
b
100 nm
Low pH

Fig. 9: *AFM imaging of TRPC1*. (**a**) TRPC1 channels were identified in AFM scans (Scale bar, 500 nm) from flattened, TRPC1-containing proteoliposomes, placed onto freshly cleaved mica in saline solution as tetra-lobular structures as shown in the panel at the bottom. (**b**) The tetrameric structure can be easily distinguishable in higher magnification scans (1-2). (**c**) Cross section histograms from dashed lines in (**b**) indicate the height and diameter of the contributing monomers, and the central indentation. Two such measurements are superimposed (1-2) in the graph. (**d**) Population analysis of channel units, indicate the average diameter and height, respectively (n=105). (**e**) Analysis of the distribution of diameters indicates two peaks, suggesting asymmetry in the shape of the channels. (**f**) Further analysis of the distribution of heights indicates three peaks.

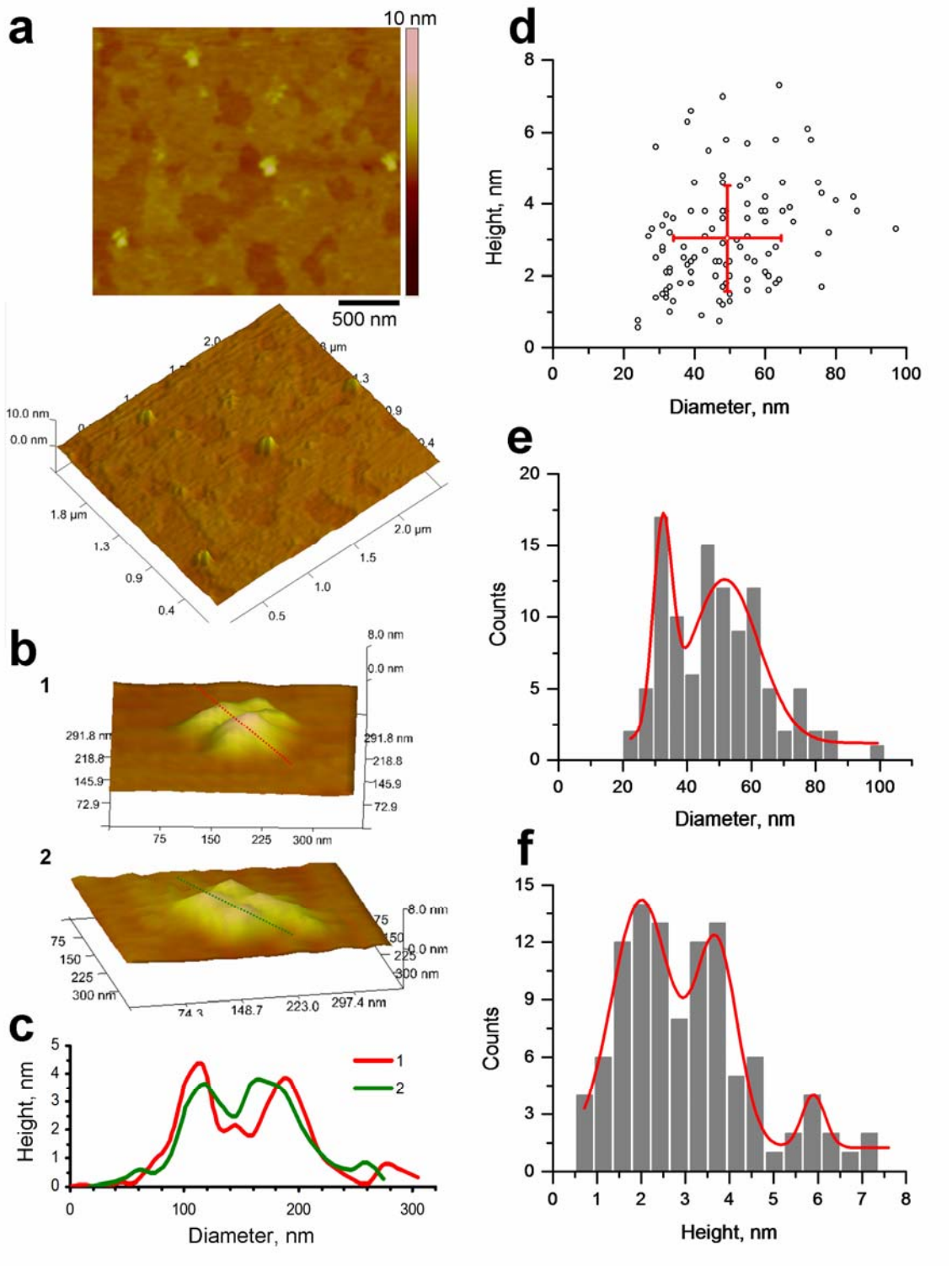
a
10 nm
500 nm
10.0 nm
0.0 nm
1.8 μm
1.3
0.9
0.4
2.0 μm
1.5
1.0
0.5
b
1
8.0 nm
0.0 nm
291.8 nm
218.8
145.9
72.9
75
150
225
300 nm
2
74.3
148.7
223.0
297.4 nm
c
Height, nm
Diameter, nm
1
2
d
Height, nm
Diameter, nm
e
Counts
Diameter, nm
f
Counts
Height, nm

Fig. 10: *Distribution of the molecular volumes of PC2 and TRPC1 homomeric complexes.* (**a**) The height-diameter relationship of PC2 (n=97). Complexes with height higher than 2 nm were excluded from analysis. A linear fitting showed no/weak linear correlation between height and diameter (R^2=0.0934). (**b**) Histogram of calculated molecular volume of PC2 molecular complexes. (**c**) Height-diameter relationship for TRPC1 (n=94). Note the complexes with height higher than 5 nm were excluded from analysis. A linear fitting also revealed no/weak correlation between height and diameter (R^2=0.161). (**d**) Histogram of calculated molecular volumes of TRPC1 complexes.

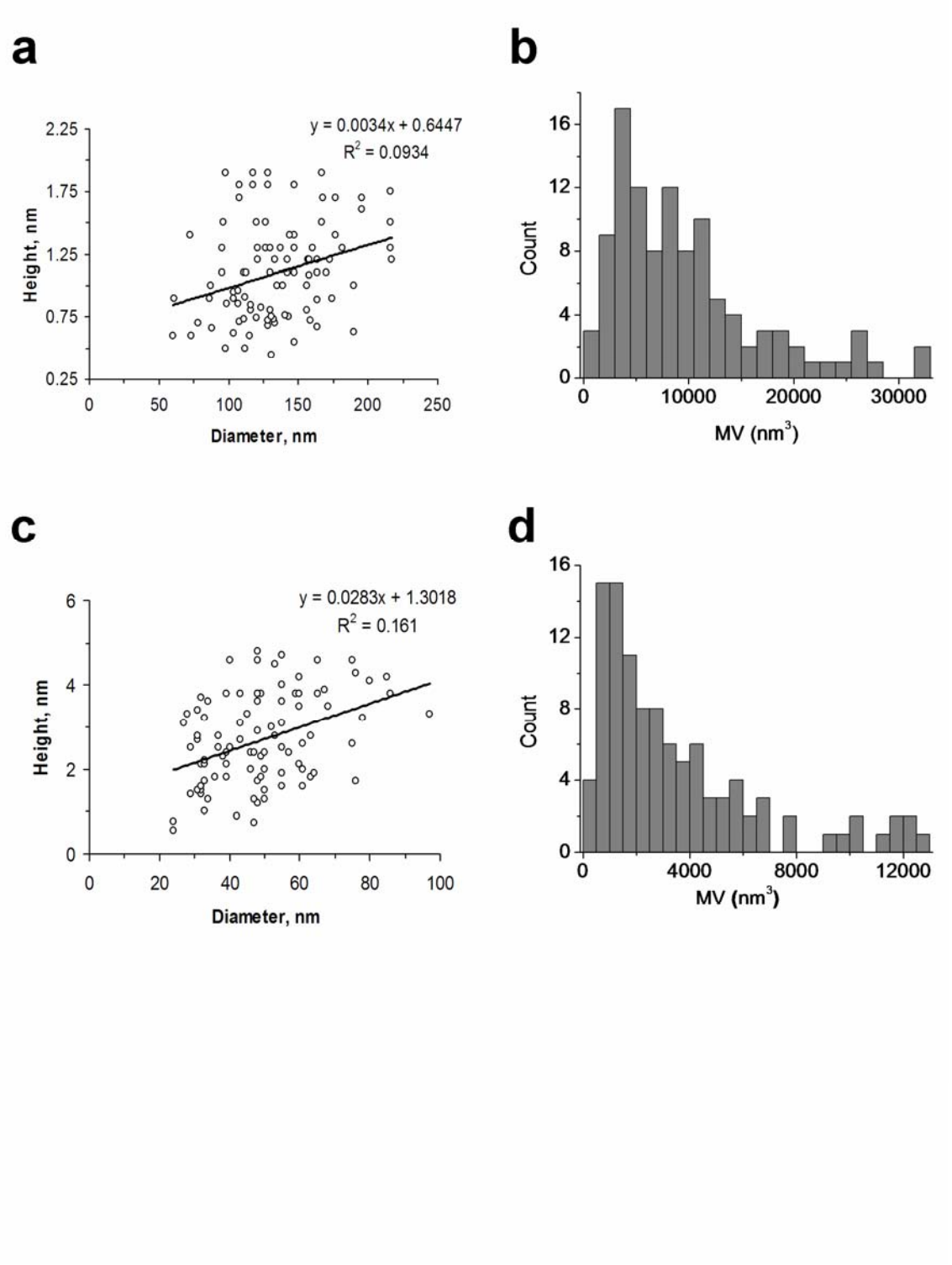
a
y = 0.0034x + 0.6447
R2 = 0.0934
Height, nm
Diameter, nm
b
Count
MV (nm3)
c
y = 0.0283x + 1.3018
R2 = 0.161
Height, nm
Diameter, nm
d
Count
MV (nm3)

Fig. 11: *AFM imaging of PC2/TRPC1 hetero-complexes*. (**a**) PC2/TRPC1 hetero-multimers were prepared by mixing (1:1) affinity purified PC2 and TRPC1 proteins, which were incorporated into liposomes. PC2/TRPC1-containing proteoliposomes were placed and flattened onto freshly cleaved mica in saline solution. The amplitude (left), height (middle) and the perspective (right) images show the structure of both lipid and channel complexes at low magnification. (**b**) The height (left) and perspective (right) images at high magnification show that the hetero-multimeric channel complexes displayed lax, tetra-lobular shapes. These PC2/TRPC1 channel complexes had four contributing lobules of different height and a central indentation. The circles are examples of PC2/TRPC1 hetero-tetramers; the squares and hexagons highlight the TRPC1 homo-tetramer and PC2 homo-tetramer, respectively. (**c**) The height and diameter of the monomeric units in the PC2/TRPC1 channel complex could be easily identified in the cross section histograms (insert, dashed lines). The higher peak correlates with TRPC1 monomer, while the lower peak with PC2 monomer.

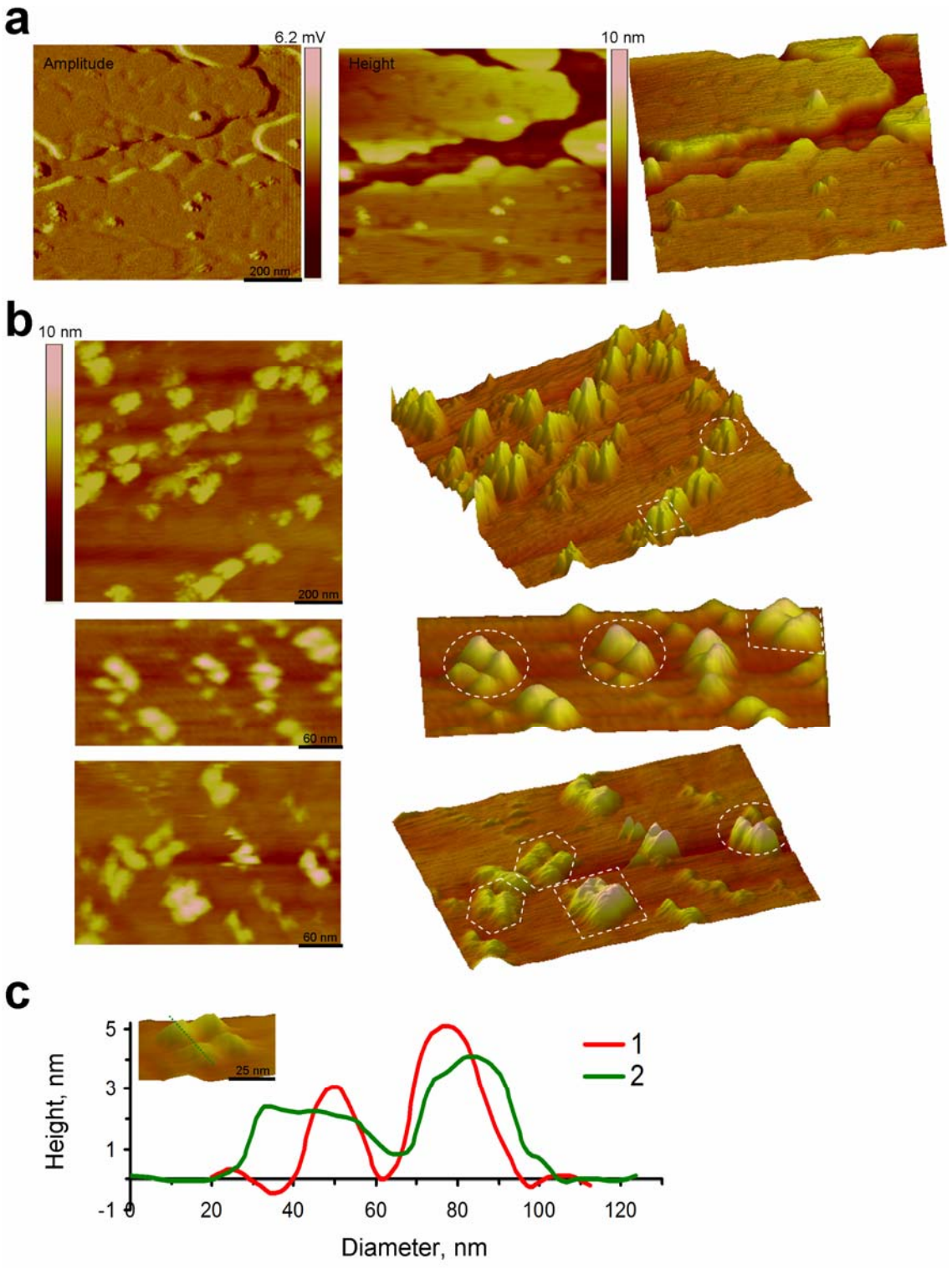
a
6.2 mV
Amplitude
200 nm
10 nm
Height
b
10 nm
200 nm
60 nm
60 nm
c
25 nm
Height, nm
5
3
1
-1
0
20
40
60
80
100
120
Diameter, nm
1
2

Abbreviations

ADPKD, autosomal dominant polycystic kidney disease; TRP, transient receptor potential, TRP, transient receptor potential; TRPC1, TRP-canonical 1; TRPP2, TRP-polycystin-2 (PC2); TRPV, vanilloid receptor; BSA, bovine serum albumin; EGTA, [ethylene-bis-(oxythylene-nitrilo)] tetraacetic acid; HEPES, 4-(2-hydoxyethyl)-1-piperazeneethanesulphonic acid.